

Interaction quantum quenches in the one-dimensional Fermi-Hubbard model with spin imbalance

L. Riegger,^{1,2} G. Orso,³ and F. Heidrich-Meisner¹

¹*Department of Physics and Arnold Sommerfeld Center for Theoretical Physics,
Ludwig-Maximilians-Universität München, D-80333 München, Germany*

²*Max-Planck-Institute of Quantum Optics, D-85748 Garching, Germany*

³*Laboratoire Matériaux et Phénomènes Quantiques,
Université Paris Diderot-Paris 7 and CNRS, UMR 7162, 75205 Paris Cedex 13, France*

Using the time-dependent density matrix renormalization-group method and exact diagonalization, we study the nonequilibrium dynamics of the one-dimensional Fermi-Hubbard model following a quantum quench or a ramp of the on-site interaction strength. We are particularly interested in the nonequilibrium evolution of Fulde-Ferrell-Larkin-Ovchinnikov (FFLO) correlations, which, at finite spin polarizations and for attractive interactions, are the dominant two-body correlations in the ground state. For quenches from the noninteracting to the attractive regime, we investigate the dynamical emergence of FFLO correlations and their signatures in the pair quasi-momentum distribution function. We observe that the postquench double occupancy exhibits a maximum as the interaction strength becomes of the order of the bandwidth. Finally, we study quenches and ramps from attractive to repulsive interactions, which imprint FFLO correlations onto repulsively bound pairs. We show that a quite short ramp time is sufficient to wipe out the characteristic FFLO features in the postquench pair momentum distribution functions.

I. INTRODUCTION

The physics of low-dimensional Fermi gases with attractive interactions and unequal spin populations has generated interest because of the possibility of realizing exotic fermionic superfluids such as the Sarma [1] and Fulde-Ferrell-Larkin-Ovchinnikov (FFLO) states [2, 3] (see Refs. [4–6] for a review). The FFLO state is characterized by a spatially oscillating order parameter with the excess fermions sitting mainly in its nodes, where they are less detrimental to superconductivity. The FFLO state is currently invoked to explain the behavior of several superconducting systems, ranging from heavy fermion [7] and organic [8] materials to dense quark matter in the core of neutron stars [9]. However, the experimental evidence of this phase in solid-state superconductors is still controversial. In particular, the one-dimensional (1D) analog of the FFLO state, a state with spatially oscillating pairing correlations is, at a finite spin imbalance, the ground state of the Fermi-Hubbard model and its continuum analog, the Yang-Gaudin model (see Refs. [10] and [11] for a review). A recent experiment [12] has realized a spin-imbalanced Fermi gas in an array of 1D systems and has demonstrated that the observed density profiles are in agreement with theoretical predictions [13–15]. An actual experimental proof of the presence of a spatially modulated quasicondensate in this system, expected from theory [16–21], is still lacking, which has led to a large number of proposals for schemes to probe FFLO correlations [22–27]. Many of these proposals involve the presence of an optical lattice along the 1D direction, suggesting that the Fermi-Hubbard model is the appropriate model. This system has been realized with ultracold atoms by several groups [28–30].

One-dimensional gases also provide a natural arena for the study of the nonequilibrium dynamics of closed,

strongly correlated many-body systems and several experiments were specifically tailored to explore this physics [31–38]. For instance, theoretical and experimental research is aiming at understanding the conditions for the emergence of thermalization [39, 40] and the qualitative features in the relaxation dynamics such as time scales for the approach to the steady state (see Refs. [40–42] for recent reviews). Integrable 1D models such as the Fermi-Hubbard model play a special role, since there, thermalization can often only occur with respect to so-called generalized Gibbs ensembles [43], a subject addressed in a series of recent studies (see, e.g., [44–50]).

In this work we study the real-time dynamics of FFLO correlations and the double occupancy in interaction quantum quenches in the Fermi-Hubbard model with spin imbalance. The Hamiltonian of the system is given by

$$H = -J \sum_{i=1}^{L-1} (c_{i\sigma}^\dagger c_{i+1\sigma} + h.c.) + U \sum_{i=1}^L n_{i\uparrow} n_{i\downarrow}, \quad (1)$$

where $c_{i\sigma}$ annihilates a fermion with spin $\sigma = \uparrow, \downarrow$ at site i of a chain of length L , $n_{i\sigma} = c_{i\sigma}^\dagger c_{i\sigma}$ is the density operator for the spin- σ component, U is the on-site interaction and J , the hopping parameter. Moreover, we define the total density, $n = (N_\uparrow + N_\downarrow)/L$, and the spin polarization, $p = (N_\uparrow - N_\downarrow)/(N_\uparrow + N_\downarrow)$, N_σ being the number of particles with spin σ . The nonequilibrium dynamics in the Fermi-Hubbard model has been studied in recent experiments [51–54]. Our main interest is in the relaxation dynamics, the identification of relevant time scales for the formation of FFLO correlations, and the dependence of observables on postquench parameters.

Based on two numerical methods, time evolution in a Krylov subspace using exact diagonalization (ED; see, e.g., [55] and [56]) and the time-dependent version of

the density matrix renormalization-group (DMRG) technique [57–59], we investigate the behavior of the system following both instantaneous and slow quenches of the interaction strength. In the latter case, we are interested in the crossover to the adiabatic regime (see Refs. [60] and [61] for studies of slow quenches in the Bose-Hubbard model).

We first present results for quenches from the noninteracting case, $U = 0$, to the attractive regime, $U < 0$. In particular, we investigate how FFLO correlations emerge in the system and we propose that a time scale can be extracted by monitoring the dynamics of natural orbitals, which are the eigenstates of the pair density matrix, and of the pair quasi-momentum distribution function (MDF). The latter quantity is a key observable in the discussion of the FFLO state since the spatially inhomogeneous quasicondensate translates into maxima in the pair MDF at finite momenta q , which is controlled via the polarization [10, 17]

$$q = \pi np. \quad (2)$$

Moreover, we analyze the relaxation dynamics of the double occupancy, a much discussed quantity in studies of quantum quenches in the repulsive Fermi-Hubbard model [62–71], which has been measured in nonequilibrium experiments [29, 37, 51].

We then turn our attention to quenches from the attractive regime, $U < 0$, to the repulsive one, $U > 0$. In particular, we demonstrate how FFLO correlations of Cooper pairs can be imprinted onto repulsively bound pairs. We find that the visibility of the FFLO peak crucially depends on the final (postquench) value of U and on the ramp time.

The plan of this paper is as follows. In Sec. II, we introduce the quench schemes and provide definitions of quantities used throughout the paper and details on our numerical methods. Section III is devoted to the formation of FFLO correlations in quenches and ramps starting from the noninteracting case to negative values of U . In Sec. IV, we discuss the imprinting of FFLO correlations onto repulsively bound pairs in quenches and ramps from $U < 0$ to $U > 0$. In Sec. V, we summarize our main results and discuss perspectives for future work on this exciting topic.

II. SET-UP, DEFINITIONS, AND METHODS

A. Quench schemes

We consider two quench schemes. In the first case, we prepare the system in the ground state of Eq. (1) at $U = 0$, and at $t = 0$ we change the interaction strength to $U < 0$. This probes the formation of FFLO correlations in a previously noninteracting two-component Fermi gas. In the second scheme, the initial state is the ground state at some $U < 0$, and then we instantaneously change the

sign of the interaction at $t = 0$. This scheme is supposed to imprint FFLO correlations onto the repulsively bound pairs present on the repulsive side $U > 0$.

Besides these quenches that change the value of U abruptly from U_i to U_f , we also consider slow, linear quenches, referred to as ramps, where in the time interval $t \in [0, t_{\text{ramp}}]$, U takes the time dependence according to

$$U(t) = U_i + \frac{U_f - U_i}{t_{\text{ramp}}} t, \quad (3)$$

where t_{ramp} is the ramp time.

B. Observables

Our study mainly focuses on two quantities, namely, the double occupancy and the pair MDF. The double occupancy d is defined as

$$d = \sum_{i=1}^L \langle n_{i\uparrow} n_{i\downarrow} \rangle. \quad (4)$$

The pair MDF n_k^{pair} (MDF) is the Fourier transform of pair correlations $\rho_{\ell j}^{\text{pair}}$, where

$$\rho_{\ell j}^{\text{pair}} = \langle c_{\ell\uparrow}^\dagger c_{\ell\downarrow}^\dagger c_{j\downarrow} c_{j\uparrow} \rangle \quad (5)$$

such that

$$n_k^{\text{pair}} = \frac{1}{L} \sum_{\ell, j} e^{i(\ell-j)k} \rho_{\ell j}^{\text{pair}}. \quad (6)$$

Note that the two quantities defined above are related to each other by the normalization condition $d = \sum_k n_k^{\text{pair}}$.

While generally, there are established methods to measure the MDF of the fermionic components via time-of-flight and band-mapping techniques [72], the measurement of the pair MDF in the FFLO phase has not been accomplished yet, but its observation is the goal of future experiments [12].

We further define the visibility V via

$$V = \frac{n_{k=q}^{\text{pair}} - n_{k=0}^{\text{pair}}}{n_{k=q}^{\text{pair}} + n_{k=0}^{\text{pair}}}. \quad (7)$$

This particular definition is motivated by the fact that the maximum in n_k^{pair} is initially at $k = 0$ for $U_i = 0$ and at $k = \pm q$ in the ground state for $U < 0$.

C. Numerical methods

We employ two numerical methods in our work, namely, ED and the DMRG method [57–59]. In the ED method, we use a Krylov-space method to propagate the wave function in time (for technical details, see,

e.g., [55]). We use a Trotter-Suzuki method to propagate the wave function using the DMRG; the time step is typically chosen to be $\delta t \sim 0.02/J$. The discarded weight, which controls the accuracy of the truncation involved in the DMRG [73, 74], is set to 10^{-6} , which is sufficient to ensure negligible numerical errors for the times reached in the simulation. We perform all DMRG and ED simulations for open boundary conditions.

III. FORMATION OF FFLO CORRELATIONS IN QUENCHES AND LINEAR RAMPS FROM $U = 0$ TO $U < 0$

In this section, we present our results for quenches and linear ramps from the noninteracting case $U_i = 0$ to attractive interactions $U_f < 0$. First, we discuss the behavior of the double occupancy and the pair MDF for the quantum quench in Sec. III A and then we turn to slow quenches in Sec. III B.

A. Quantum quench

1. Double occupancy

Example for time evolution. Typical results for the time dependence of the double occupancy are shown in Fig. 1(a), where we display ED data for $L = 12$ and DMRG data for $L = 24, 36$, $U_f = -8J$, polarization $p = 1/2$, and filling $n = 1/3$. Since the system is initially prepared in an uncorrelated state, the double occupancy at $t = 0$ is given by $d(0) = n_{\uparrow}n_{\downarrow}L$; that is,

$$\frac{d(0)}{N_{\downarrow}} = \frac{n(1+p)}{2}. \quad (8)$$

Similarly to the behavior of the double occupancy in other interaction quantum quenches [37, 75], $d(t)$ undergoes a fast transient characterized by large oscillations and relaxes to a constant value \bar{d} on a time scale τ_d of order $1/J$, as is evident from the data for $L = 36$. For small systems such as $L = 12$, there are revivals due to reflections from the boundary of the simulation box. These spurious oscillations quickly disappear as L increases.

Long-time average \bar{d} . We extract the stationary value \bar{d} by averaging the double occupancy $d(t)$ at long times ($t \gtrsim 3/J$). These data are plotted in Fig. 2 as a function of the postquench interaction strength U_f/J for two values of the filling, namely, $n = 1/3$ and $n = 2/3$, and polarization $p = 1/2$. As $|U_f|/J$ increases, we see that initially \bar{d} increases from its $U = 0$ value until it reaches a maximum value as the interaction strength becomes of the order of the bandwidth, $|U_f|/J \sim 4$, and then it decreases (slowly) for larger values of $|U_f|$.

It is instructive to compare the steady-state double occupancy \bar{d} to its ground-state value d_{gs} , calculated for $U = U_f$. The latter is shown in Fig. 2 by dashed lines.

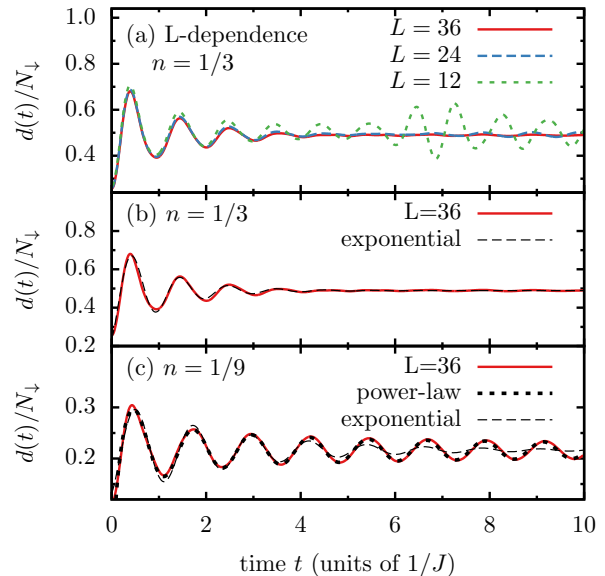


FIG. 1. (Color online) (a) System-size dependence [lattice sizes $L = 12$ (ED), $L = 24, 36$ (DMRG)] of the time evolution of the double occupancy $d(t)/N_{\downarrow}$ after the interaction quench from $U_i = 0$ to $U_f = -8J$ at $n = 1/3$, $p = 1/2$. (b) Fit (dashed black line) of a single, exponentially damped oscillation $-a \cos(\omega t + \phi) \exp(-t/\tau_d) + \bar{d}$ to the dynamics of $d(t)$ [for $t \lesssim 3/J$: $\tau_d = (1.05 \pm 0.02)/J$, $\omega = (6.15 \pm 0.02)J$, \bar{d} from $t > 3/J$]. Note that we observe a short relaxation time, $\tau_d \sim 1/J$, for this set of parameters. (c) $d(t)$ at low densities. In this regime, the relaxation follows a power-law (dotted black line), $-a \cos(\omega t + \phi)/t^{\alpha} + \bar{d}$ [for $0.1/J \lesssim t \lesssim 5/J$: $\alpha = 0.53 \pm 0.01$, $\omega = (5.097 \pm 0.005)J$] and cannot be described by the fit of an exponentially damped oscillation (dashed black line).

Different from \bar{d} , the ground-state double occupancy is a monotonically increasing function of $|U|/J$, approaching the largest possible value of $d_{\text{gs}} = N_{\downarrow}$ for $|U|/J \rightarrow \infty$ (note that we plot the ratio \bar{d}/N_{\downarrow} in the figure). In particular, taking into account that $d_{\text{gs}} = \partial E_{\text{gs}}/\partial U$, where $E_{\text{gs}} = -\sqrt{U^2 + 16J^2}$ is the ground-state energy of the two-body problem, for vanishing density, $n \rightarrow 0$, we find (dotted line in Fig. 2)

$$\frac{d_{\text{gs}}}{N_{\downarrow}} = \frac{-U}{\sqrt{U^2 + 16J^2}}. \quad (9)$$

We see in Fig. 2 that for sufficiently weak interactions, $|U_f| \ll J$, the steady-state double occupancy follows closely the postquench ground-state value, while for stronger interactions it is well below that value. This effect can be understood by taking into account that during the time evolution the energy is conserved, i.e.,

$$E_{\text{kin}}(0) + U_f d(0) = E_{\text{kin}}(t) + U_f d(t), \quad (10)$$

where E_{kin} is the expectation value of the kinetic energy. Equation (10) shows that an increase in the double

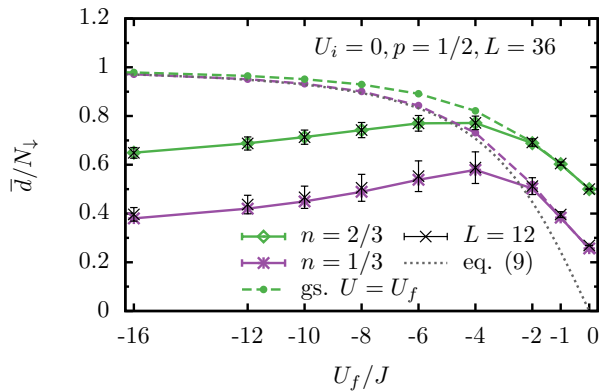


FIG. 2. (Color online) Time average \bar{d} of the double occupancy $d(t)$ versus the postquench interaction strength U_f after the quench from $U_i = 0$, for different fillings, $n = 2/3$ (diamonds) and $n = 1/3$ (asterisks), for $L = 36$ (DMRG). Black X's indicate the corresponding results for $L = 12$ (ED). Dashed lines show the ground-state values for $U = U_f$. Error bars indicate the standard deviation from the mean value (not visible for $L = 36$). The dotted line shows the result for the low-density limit, Eq. (9).

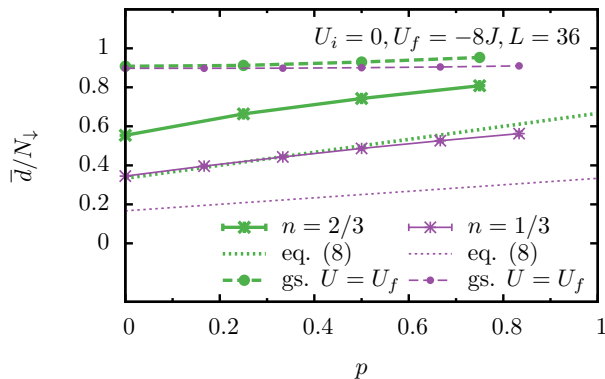


FIG. 3. (Color online) Time average \bar{d} of the double occupancy after the quench from $U_i = 0$ to $U_f = -8J$ as a function of the polarization p . Thin and thick lines correspond to fillings $n = 1/3$ and $n = 2/3$, respectively. Dotted lines show the prequench value of \bar{d} from Eq. (8); dashed lines indicate the postquench ground-state value with $U = U_f$. All data for $L = 36$ (DMRG); the time average was computed for $t > 3/J$.

occupancy has to be compensated by a corresponding change in the kinetic energy. Since the single-particle dispersion has a finite bandwidth $4J$, the conversion between interaction and kinetic energies is progressively inhibited for $|U_f| > 4J$, implying that \bar{d} decreases by further increasing the interaction strength. In particular, for $U_f/J \rightarrow -\infty$ the double occupancy remains frozen to its initial value, $\bar{d} = d(t) = d(0)$, with the latter given by Eq. (8).

In Fig. 3, we show the dependence of \bar{d} on the spin polarization for fixed interaction strength $U_f = -8J$ and

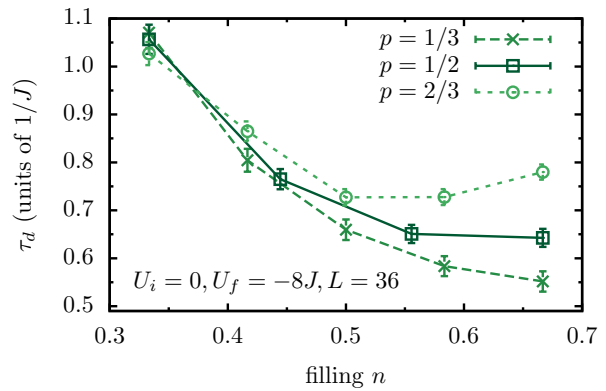


FIG. 4. (Color online) Relaxation time τ_d of the double occupancy in the quench from $U_i = 0$ to $U_f < 0$ versus filling n for different polarizations p and $U_f = -8J$ ($L = 36$; DMRG). Error bars indicate the asymptotic standard error from the least-squares fit of Eq. (11) to the data.

for two fillings, $n = 2/3$ (diamonds) and $n = 1/3$ (asterisks). \bar{d} increases roughly linearly as a function of p , as is the case for the initial double occupancy [see Eq. (8)].

Relaxation towards the stationary regime. To further analyze the data, we observe that the fit function

$$d(t) = -a \cos(\omega t + \phi) \exp(-t/\tau_d) + \bar{d} \quad (11)$$

provides a reasonably good description of the numerical data in a wide parameter regime. An example is shown in Fig. 1(b) for the largest system size, $L = 36$.

The frequency of the coherent oscillation is, for large values of $|U_f|/J$, given by $\omega \propto |U_f|$, similar to other studies of collapse and revival phenomena [53, 76, 77], since the dynamics is predominantly governed by the interaction term in that limit. By the same argument, ω increases with density, since the double occupancy increases with density, both at equilibrium and in the steady state. In the two-body limit ($N_{\uparrow} = N_{\downarrow} = 1$), the frequency is given by the binding energy ϵ_b :

$$\omega = \epsilon_b = \sqrt{U^2 + 16J^2} - 4J. \quad (12)$$

In particular, the good agreement between Eq. (11) and the data shown in Fig. 1(b) suggests that there is an exponential decay towards the time-independent value \bar{d} , which allows us to extract the relaxation time τ_d .

We observe that τ_d varies only mildly with both polarization and postquench interaction strength U_f , whereas the dependence on n is much stronger. This is illustrated in Fig. 4, where we plot τ_d versus n . Starting at low densities, τ_d decreases as n increases and then becomes as short as $\tau_d \sim 0.5/J$. For large polarizations, however, τ_d increases again for $n \rightarrow 1$. Several aspects play a role in the relaxation dynamics: (i) the presence of doublons defined by the initial state at $t = 0$, (ii) the formation of additional doublons and (iii) the scattering of doublons, which leads to the decay of $d(t)$ to the stationary value.

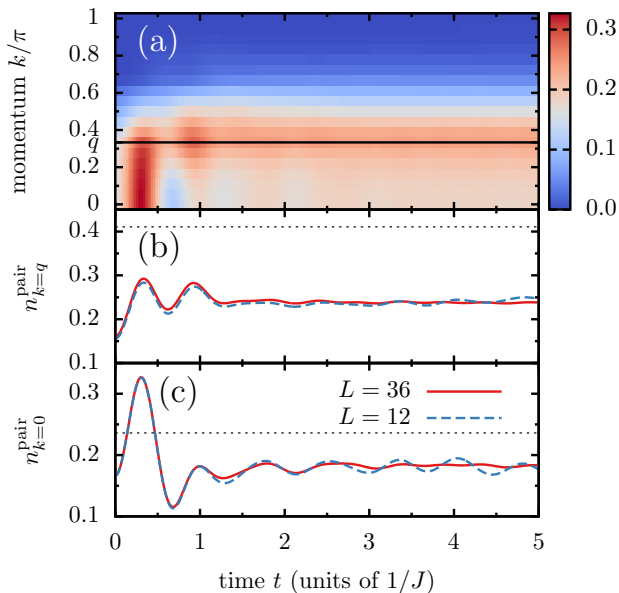


FIG. 5. (Color online) (a) Pair momentum distribution $n_k^{\text{pair}}(t)$ after the interaction quench from $U_i = 0$ to $U_f = -8J$ at $n = 1/3$, $p = 1/2$, $L = 36$ (DMRG); the horizontal line marks the position of the FFLO momentum q set by the density and polarization. (b) $n_{k=q}^{\text{pair}}(t)$ at the FFLO momentum q . (c) $n_{k=0}^{\text{pair}}(t)$ at zero momentum; solid lines for $L = 36$ (DMRG) and dashed lines for $L = 12$ (ED). Dotted horizontal lines in (b) and (c) indicate postquench ground-state values of the respective variables.

The density dependence can be understood from the simple argument that the higher the density, the higher is the probability of scattering events. At a high density, these events can occur on times scales set by the inverse hopping rate, resulting in $\tau_d \sim 1/J$.

In the opposite limit of low densities $n \lesssim 0.2$, the decay of the amplitude of the oscillations is actually better described by a power-law than by an exponential. This is illustrated in Fig. 1(c), where the fits to both a power law and an exponential relaxation are shown. One can therefore attempt to describe the crossover from a power-law, realized at small n , to an exponential relaxation at large n with a function

$$d(t) = -a \cos(\omega t + \phi) \exp(-t/\tau_d)/t^\alpha + \bar{d}. \quad (13)$$

Therefore, the power-law decay and the coherent oscillations are inherited from the few-body dynamics, whereas the many-body physics introduces an actual damping. Consistent with this picture, we observe that the exponent of the power-law $\alpha \approx 0.5$ very weakly depends on U_f/J and that τ_d becomes very large for $n \rightarrow 0$.

2. Pair correlations and quasi-momentum distribution function

Time evolution of the pair MDF. We next turn to the main quantity of interest in our study, namely the pair MDF n_k^{pair} . A typical example of its time evolution in the quench from $U_i = 0$ to $U_f = -8J$ is shown in Fig. 5(a). At $t = 0$, there is a maximum at $k = 0$, which, after the quench and a fast transient time that is shorter than $1/J$, moves to finite momenta and then approaches $k = q$, where q is given by Eq. (2).

From its definition, Eq. (6), it follows that the pair MDF is normalized to the double occupancy $\sum_k n_k^{\text{pair}} = d$. Since the quench both introduces a redistribution of weight and generates additional pairs, as is evident in Fig. 2, the sum over n_k^{pair} increases. Figures 5(b) and 5(c) show the individual time evolution of $n_{k=q}^{\text{pair}}$ and $n_{k=0}^{\text{pair}}$, respectively. Both numbers are always below the expectation values in the postquench ground state (dotted lines). There are only small finite-size effects, comparing $L = 12$ (dashed lines) and $L = 36$ (solid lines). Compared to its initial value at $t = 0$, the long-time average of $n_{k=0}^{\text{pair}}$ does not decrease much (this can be different for other parameter values), while $n_{k=q}^{\text{pair}}$ increases significantly. In any case, the largest absolute increase in n_k^{pair} typically occurs at $k = q$ (compare also Fig. 10).

Natural orbitals and decay of correlations. In order to further characterize the state after the fast quench dynamics, it is instructive to compute the natural orbitals $\phi_\mu(i)$, which are the eigenvectors of the pair-pair correlation function ρ_{ij}^{pair} defined in Eq. (5). We are, in particular, interested in the spatial structure of the natural orbital $\phi_0(i)$ that belongs to the largest eigenvalue of ρ_{ij}^{pair} . The time average of this state [i.e., the time average over $|\phi_0(i)|^2$] is plotted in Fig. 6(a), compared to the same quantity in the postquench and prequench ground state (all for $U_f = -8J$). As expected we observe a spatial oscillation with $k = q$ that was not present in the initial state (diamonds). The amplitude in the time-averaged state is smaller than in the postquench ground state (squares).

The pair correlation function ρ_{ij}^{pair} itself, shown in Fig. 6(b), has a power-law decay in the postquench ground state superposed with oscillations [16, 17]. The same characteristic FFLO oscillations emerge in the time-averaged postquench state, yet the decay of the spatial correlations is much faster and roughly exponential.

From these results, we conclude that the time-averaged state indeed has the characteristic features of the FFLO state, albeit not with quasi-long-range order, which is expected since the system is at a finite energy above the ground state. Our next goal is to define and analyze a characteristic time scale for the formation of the FFLO correlations.

Time scale for the formation of FFLO correlations. In contrast to the double occupancy, $n_k^{\text{pair}}(t)$ does not ex-

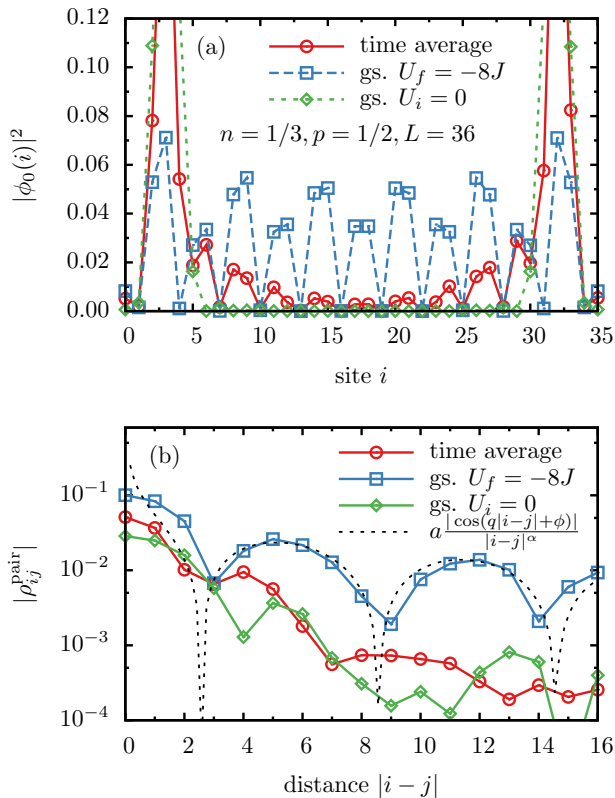


FIG. 6. (Color online) (a) Lowest natural orbital $|\phi_0(i)|^2$ in the ground state of the noninteracting system ($U_i = 0$; diamonds), and in the ground state of the attractively interacting system ($U_f = -8J$; squares), and time average (for $t > 3/J$) after the initial quench dynamics (circles). (b) Time-averaged spatial decay (circles) of pair-pair correlations $|\rho_{ij}^{\text{pair}}|$ after a quench from $U_i = 0$ to $U_f = -8J$ (circles; time averages calculated for $t > 3/J$), in the ground state of the noninteracting system ($U = 0$; diamonds), and in the ground state of the attractively interacting system ($U = -8J$; squares). Dotted line: Fit of $f(|i-j|) = a \frac{|\cos(q|i-j|+\phi)|}{|i-j|^\alpha}$ to the $U = -8J$ ground state for $|i-j| \geq 3$, with q taken from the position of the maximum in the pair-momentum distribution and fitting parameters a , α , and ϕ . All data are for $n = 1/3$, $p = 1/2$, and $L = 36$ (DMRG).

hibit a single relaxation time, i.e., it is not well approximated by a simple fit function of the type of Eq. (11). In order to, nevertheless, define a time scale for the formation of FFLO correlations, we find it instructive to study the time evolution of the natural orbital $\phi_0(i)$. This quantity is shown in Fig. 7(a). Initially, apart from oscillations in $|\phi_0(i)|^2$ induced by the open boundaries, $\phi_0(i)$ is flat, yet at times $t \sim 0.5J$, it clearly develops a spatially modulated pattern, indicative of FFLO correlations.

The time τ_{FFLO} at which this modulation appears in $|\phi_0(i)|^2$ is also reflected in the time dependence of the visibility $V(t)$ of the FFLO peak in n_k^{pair} defined in Eq. (7), namely, for $t \lesssim \tau_{\text{FFLO}}$, $V(t) < 0$ while for $t \gtrsim \tau_{\text{FFLO}}$, $V(t) > 0$, as is evident from Fig. 7. We therefore de-

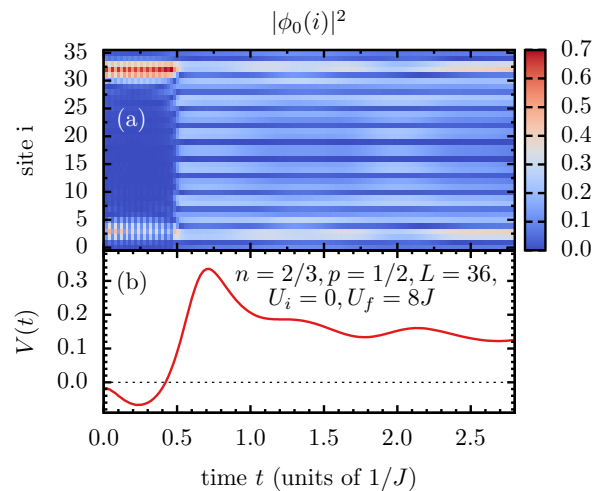


FIG. 7. (Color online) (a) Time evolution of the lowest natural orbital $|\phi_0(i)|^2$ [for better color contrast, we plot $|\phi_0(i)|$] and (b) time evolution of the FFLO visibility V [see Eq. (7)]. The time at which the natural orbital $|\phi_0(i)|^2$ develops an oscillatory pattern roughly coincides with the time at which the visibility goes through 0. For the prequench system with $U_i = 0$ the lowest natural orbital is twofold degenerate, where one of them has a deviation from the constant background near the left, and the other near the right, boundary. Numerically, we select one of the degenerate orbitals, which explains the spatial anisotropy of $|\phi_0(i)|^2$ for $t \lesssim \tau_{\text{FFLO}}$. All data for $n = 2/3$, $p = 1/2$, and $L = 36$ (DMRG).

fine the time scale characteristic for the formation of the FFLO correlations as the (first) 0 of the visibility,

$$V(\tau_{\text{FFLO}}) = 0. \quad (14)$$

Note that this could be measured in experiments, provided the pair MDF is accessible.

Our results for the dependence of τ_{FFLO} on filling, polarization, and postquench interaction strength are summarized in Figs. 8(a), 8(b), and 8(c), respectively. The overall density dependence is similar to that of τ_d discussed in Sec. III A 1 (compare Fig. 4): starting from low densities, τ_{FFLO} decreases. It also monotonously decreases with p , yet exhibits a weaker overall variation.

The processes behind the formation of the FFLO correlations and the formation of the oscillatory structure in the natural orbital $|\phi_0(i)|^2$ are the pair formation, redistribution of momentum among pairs, and spatial redistribution of excess fermions. The time scale for pair formation is similar to that for the formation of doublons [in excess of those present in the initial state; see Eq. (8)], which are essentially a measure of the pairs, while the excess fermions have to rearrange themselves over distances of $l \sim 1/(2q)$.

The probability of a minority fermion finding an excess fermion is proportional to the density of majority fermions $n_\uparrow = N_\uparrow/L$. Therefore, we expect a leading dependence for the formation of additional pairs given by $\tau_{\text{FFLO}} \propto 1/n_\uparrow = \frac{1}{n(1+p)}$. Our numerical results for τ_{FFLO}

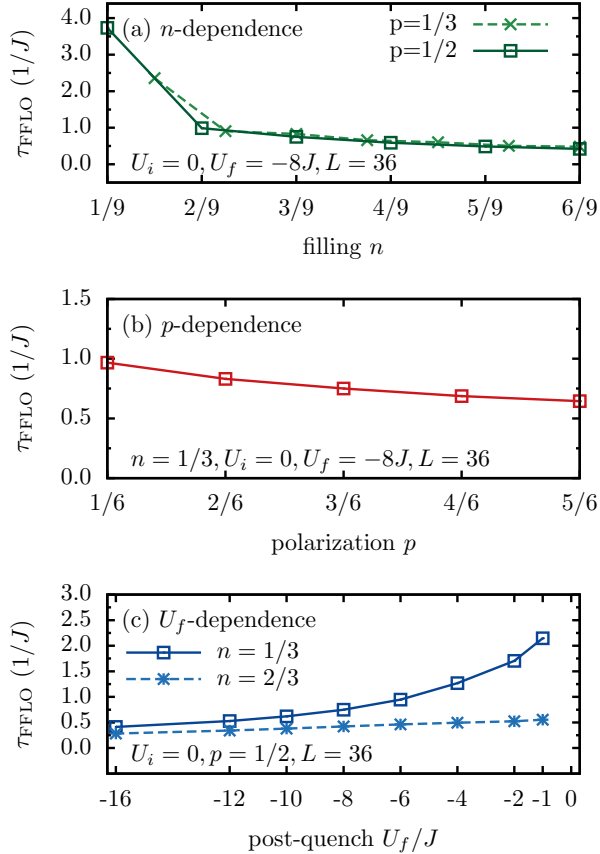


FIG. 8. (Color online) Time scale τ_{FFLO} for the formation of FFLO correlations in the quench from $U_i = 0$ to $U_f < 0$, versus (a) filling n , (b) polarization p , and (c) postquench interaction strength U_f , all for $L = 36$ (DMRG). The time scale is extracted as the first 0 of the visibility $V(t)$.

extracted from the 0 of the visibility shown in Fig. 8 are in reasonable qualitative agreement with this simple argument.

There is also an interesting dependence on U_f [see Fig. 8(c)]: (i) the smaller $|U_f|$, the larger τ_{FFLO} , and (ii) the lower the density, the more strongly τ_{FFLO} depends on U_f . The first aspect is intuitive, since for $|U_f| \rightarrow 0$, no FFLO correlations are ever formed, and hence $\tau_{\text{FFLO}} \rightarrow \infty$. Note also that for large $|U_f|/J$, τ_{FFLO} seems to become independent of the density.

Time average of the visibility. We finally discuss the long-time average of the visibility as a function of the postquench interaction strength. The results are shown in Fig. 9, for the dependence of V both on U/J in the ground state [Fig. 9(a)] and on the postquench interaction strength U_f/J [Fig. 9(b)]. In both cases, V increases monotonically with U and U_f , respectively, however, the comparison of different system sizes shows only very small variations for the time averages, while in the ground state, V increases with L . This is consistent with the fact that in the ground state we have an actual qua-

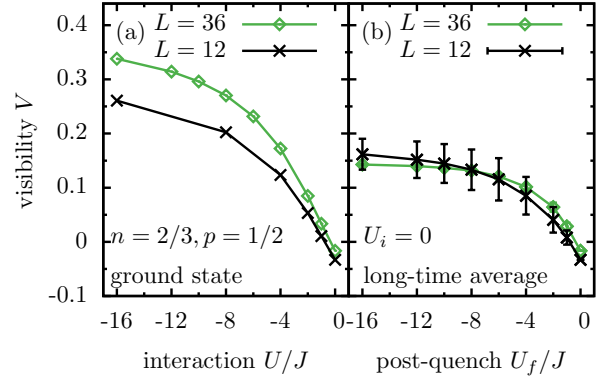


FIG. 9. (Color online) (a) Visibility V of the FFLO peak in n_k^{pair} in (a) the ground state at interaction strength U , and (b) the long-time average (calculated for $t > 3/J$) of V versus the postquench interaction strength U_f after the quench from $U_i = 0$, all for $L = 36$ (DMRG) and $L = 12$ (ED). Error bars indicate the standard deviation from the time average (not visible for $L = 36$).

sic condensate.

B. Ramps from $U = 0$ to $U < 0$: Crossover to adiabatic dynamics

To conclude our discussion of the real-time dynamics starting from a noninteracting gas, we turn to slow quenches with a linear ramp from $U_i = 0$ to U_f according to Eq. (3). We are, in particular, interested in the crossover to adiabatic behavior, for which we expect to obtain the ground-state expectation values of observables in the time average.

Our results for the time average of n_k^{pair} versus quasi-momentum k for ramps and quenches to $U_f = -8J$ are presented in Figs. 10(a), 10(b), 10(c), and 10(d) for polarizations $p = 0, 1/4, 1/2$, and $3/4$, respectively. These plots also include n_k^{pair} calculated in the ground state at $U_i = 0$ and $U_f = -8J$ and the results for instantaneous quenches. For the quenches, the time averages at $p > 0$ result in maxima at $k = q$ but the distribution is mostly reduced in height compared to the postquench ground state (squares).

Moreover, we see that, for both quenches and ramps, for large values of the quasi-momentum k , the time-averaged pair momentum distribution is already very close to its ground-state value for $U = U_f$ and therefore does not depend much on the sweep rate. For small quasi-momenta, the averaged pair momentum distribution increases by decreasing the sweep rate. Nevertheless, the comparably short ramp time of $t_{\text{ramp}} \sim 3/J$ is enough to obtain time averages that are very close to the ground-state correlations also for small quasi-momenta.

It is important to emphasize that the time-averaged pair momentum distribution, for most parameter values,

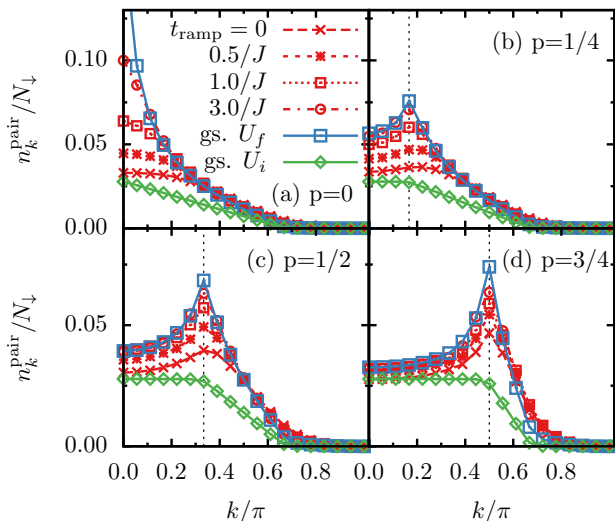


FIG. 10. (Color online) Time average of the pair-momentum distribution n_k^{pair} between $t = t_{\text{ramp}}$ and $t_{\text{max}} = 4/J$ after linear ramps from the noninteracting system ($U_i = 0$) to attractive interactions ($U_f = -8J$), for different ramp times t_{ramp} and polarizations (symbols with dotted lines): (a) $p = 0$; (b) $p = 1/4$; (c) $p = 1/2$; (d) $p = 3/4$. We also include the data for the ground state of the noninteracting system (diamonds) and the ground state of the attractively interacting system (squares). Dotted vertical lines show the maximum position at $k = q$. All results are for $n = 2/3$ and $L = 36$ (DMRG).

exhibits the typical FFLO peak at $k = q$, which is expected in the ground state for attractive interactions, $U = U_f < 0$.

C. Summary: Quenches and linear ramps from $U_i = 0$ to $U_f < 0$

As a main result of our analysis of quantum quenches from $U_i = 0$ to attractive interactions, we showed that the time average of the double occupancy has a maximum at $|U_f| \sim 4J$, while the value at small $|U_f|/J$ is close to the postquench ground-state values. At large $|U_f|/J$, the initial double occupancy simply gets frozen in on the accessible time scales. Interestingly, we observe that the approach to the stationary regime is exponential in time. This relaxation process is superimposed with coherent oscillations with $\omega \sim |U_f|$ for large $|U_f|/J$.

Even though the quantum quench puts the system at high energies, the pair MDF still develops a maximum at the characteristic FFLO momentum q . We analyzed the eigenstates of the pair density matrix ρ_{ij}^{pair} and showed that the emergence of a maximum in n_k^{pair} is accompanied by the eigenstate of ρ_{ij}^{pair} belonging to the largest eigenvalue developing a spatially oscillatory structure. This coincides with the point in time at which the visibility of the FFLO peak in n_k^{pair} becomes positive, meaning that

the maximum is at $k = q$. We therefore extracted a time scale for the formation of oscillatory pair correlations from the first 0 of the visibility. In ramps from $U_i = 0$ to $U_f < 0$, we observe that ramp times of $t_{\text{ramp}} \sim 3/J$ are enough to be adiabatic in the sense that the time average of n_k^{pair} after the ramp cannot be discerned from the postquench ground-state form of n_k^{pair} . Overall, both quenches and ramps produce the largest visibilities of the FFLO maximum in n_k^{pair} at large polarizations (compare Fig. 10).

It is tempting to relate the time averages to a temperature by comparison with thermodynamic ensembles, as is often done in studies of thermalization in interaction quantum quenches (see [75] and references therein). The Fermi-Hubbard model being integrable, we expect that an infinitely large number of Lagrange parameters (order of L many) is necessary to describe the time averages with a generalized Gibbs ensemble along the lines of [43]. While it is not the purpose of this study to clarify the validity of the generalized Gibbs ensemble for this particular quench, we note that we verified that the time averages of n_k^{pair} cannot be described by the canonical ensemble, as expected for an integrable model.

Various extensions of our analysis such as the formation of a polaron (i.e., $N_{\downarrow} = 1$), the dynamics in the low-density limit, and the dynamics starting from product states constitute interesting problems for future research. Some of these questions may permit an analytical solution and product states are commonly studied in quantum gas experiments (namely, the dynamics starting from product states in real space, see, e.g., [34, 36, 37, 54]).

For initial product states, the dynamics can be independent of the sign of U_f [52, 78], provided the observable is invariant under both a π boost and time reversal. The latter is not true for the pair MDF, and hence, the quench dynamics of n_k^{pair} can depend on the sign of U_f for certain initial product states. For instance, this happens if the distributions of spin-up and spin-down fermions in the lattice break (spatial) inversion symmetry.

IV. IMPRINTING FFLO CORRELATIONS ONTO REPULSIVELY BOUND PAIRS

By carrying out a quench from negative to positive values of U , we aim at imprinting FFLO correlations onto repulsively bound pairs present on the $U > 0$ side. In one dimension, repulsively and attractively bound pairs exist for all values of $U > 0$ and $U < 0$, respectively. Figure 11 shows a sketch of the spectrum of repulsively and attractively bound pairs. The former were observed in a seminal experiment with bosons in optical lattices [79]. We expect that, if $U_f \gg 4J$, the repulsively bound pairs will be very long-lived, implying that FFLO correlations will be preserved for a long time. This is related to the observation that in Hubbard models, the double occupancy is approximately conserved for values of U/J

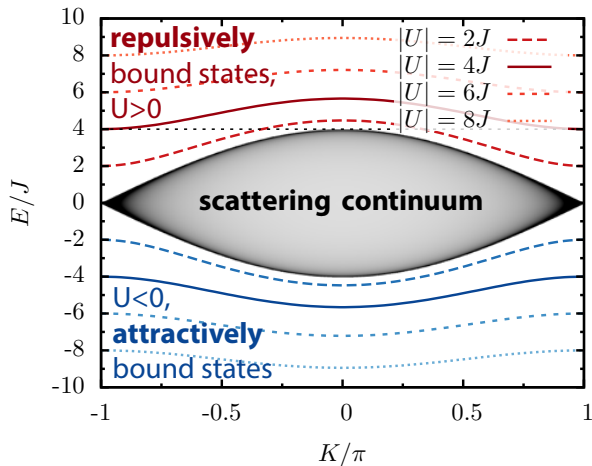


FIG. 11. (Color online) Spectra of the scattering continuum and the bound states for different on-site interaction strengths U from a two-particle calculation ($N_\uparrow = N_\downarrow = 1$) for pairs with total momentum K in the Fermi-Hubbard model. The shading of the scattering continuum is proportional to the density of states (DOS); darker gray indicates a higher DOS (note that the DOS diverges at the edges of the continuum region). The bandwidth of the scattering continuum is $8J$. Bound states are discrete and symmetric for $U \rightarrow -U$. There is no energy overlap of repulsively bound states with the continuum for $U > 4J$ (dotted black line).

larger than the band-width [80], which is at the heart of many intriguing transient and meta-stable phenomena in quantum quenches such as quantum distillation [26, 69, 81, 82] and the exponentially long thermalization times for quenches into the large- U/J regime that involve finite densities of doublons [66, 83, 84].

We first discuss quenches from $U_i < 0$ to $U_f > 0$ (Sec. IV A) and then turn our attention to linear ramps (Sec. IV B).

A. Interaction quench from $U < 0$ to $U > 0$

1. Double occupancy

On the attractive side, because of pair formation, a large double occupancy is favored, whereas $U/J > 0$ suppresses d in the ground state. The fraction of quench-induced doublons that survive in the quench from $U_i < 0$ to $U_f = |U_i| > 0$ is therefore a good measure for the stability of repulsively bound pairs. Figure 12(a) shows DMRG results for the time evolution of the relative fraction of doublons, which we define as (o representing any observable)

$$f_o(t) = \frac{o(t) - o_{\text{gs}}}{o_0 - o_{\text{gs}}}, \quad (15)$$

where o_{gs} is the expectation value in the postquench ground state and $o_0 = o(t = 0)$ is the value in the

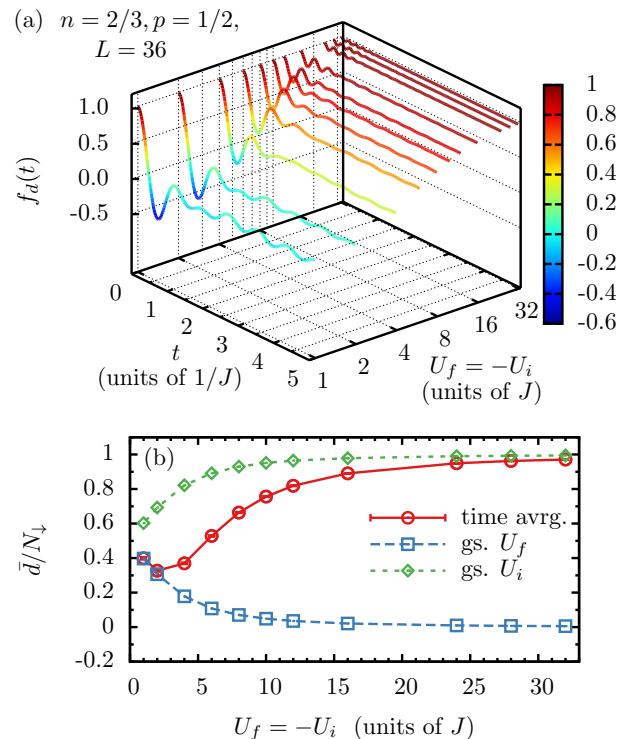


FIG. 12. (Color online) (a) Relative fraction of excess double occupancy $f_d(t)$ [see Eq. (15)] after the interaction quench from $U_i < 0$ to repulsive $U_f = |U_i| > 0$, normalized to the difference between post- and prequench ground-state values. (b) Time-averaged double occupancy \bar{d} (circles; for $t > 4/J$), postquench ground-state (squares), and initial state (diamonds) versus postquench interaction strength U_f/J . All data are for $n = 2/3$, $p = 1/2$, and $L = 36$ (DMRG).

prequench ground state. Considering $o = d$, a value of $f_d = 1$ means that all doublons survive the quench. The figure unveils that for all values of U_i , after a short transient, the double occupancy settles into a constant, superposed with oscillations. Moreover, the larger $|U_i|/J$, the more doublons survive, and $f_d \rightarrow 1$ for $|U_i|/J \gg 4$. Note that typical quantum gas experiments with interacting atoms in optical lattices reach time scales of the order of $tJ \lesssim 20$ [34], hence our results apply to the experimentally accessible time window.

Figure 12(b) shows the time average \bar{d} of the double occupancy after the quench, compared to the initial value $d(t = 0)$ and the postquench ground-state value d_{gs} . \bar{d} exceeds $d_{\text{gs}}(U_f)$ and approaches $d_{\text{gs}}(U_i)$ for $|U_i| \gg 4J$, at least on the accessible time scales. The minimum of \bar{d} at small $|U_f|/J$ has an origin similar to that of the maximum of \bar{d} in the quenches from $U_i = 0$ to $U_f < 0$ (compare Fig. 2): for low excess energies, \bar{d} is only slightly above the postquench ground-state values, but ultimately approaches the value set by the initial conditions for large $|U_f|/J$.

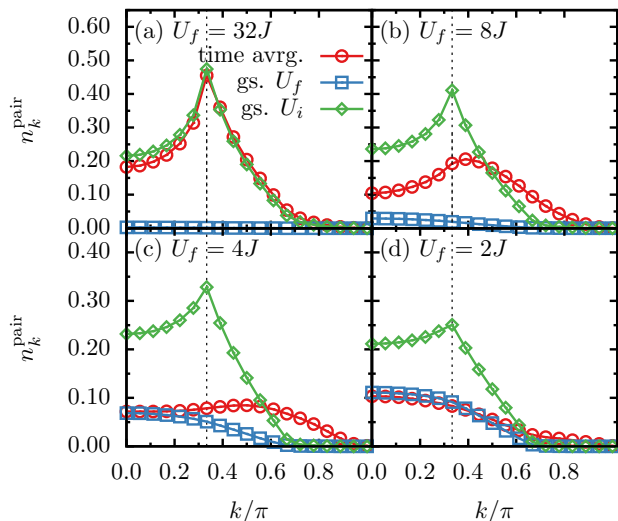


FIG. 13. (Color online) Time average of the pair momentum distribution function n_k^{pair} , calculated for $t > 3/J$, for the quench from attractive interactions $U_i < 0$ to repulsive interactions $U_f = -U_i > 0$, for different U_f —(a) $U_f/J = 32$, (b) $U_f/J = 8$, (c) $U_f/J = 4$, and (d) $U_f/J = 2$ (circles); for the ground state of the attractive system (diamonds); and for the ground state of the repulsive system at U_f (squares). All data for $n = 2/3$, $p = 1/2$, and $L = 36$ (DMRG).

2. Pair momentum distribution function

Our results for the pair MDF in the quench from $U_i < 0$ to $U_f = -U_i$ are presented in Fig. 13, which shows the time averages of n_k^{pair} versus k for the four values $U_i/J = -32, -8, -4$, and -2 at polarization $p = 1/2$ (circles). The figure also includes the respective n_k^{pair} curves in the pre- and postquench ground states (diamonds and squares, respectively). As expected, for large $|U_i|/J \gg 4$ the initial n_k^{pair} is perfectly preserved after the quench (at least for $tJ \leq 5$). Upon decreasing $|U_i|/J$, the overall height of n_k^{pair} decreases and the maximum in n_k^{pair} shifts towards larger values of $k > q$. This is related to the fact that for large quasi-momenta the time-averaged pair momentum distribution is always larger than its prequench counterpart.

As the interaction strength becomes of the order of the bandwidth, $|U_i|/J = 4$, we see that the time-averaged n_k^{pair} approaches the postquench ground-state distribution also for small momenta. By further decreasing the interaction at $|U_i|/J = 2$, the pair momentum distribution becomes already practically identical to the postquench ground-state curve for all quasi-momenta.

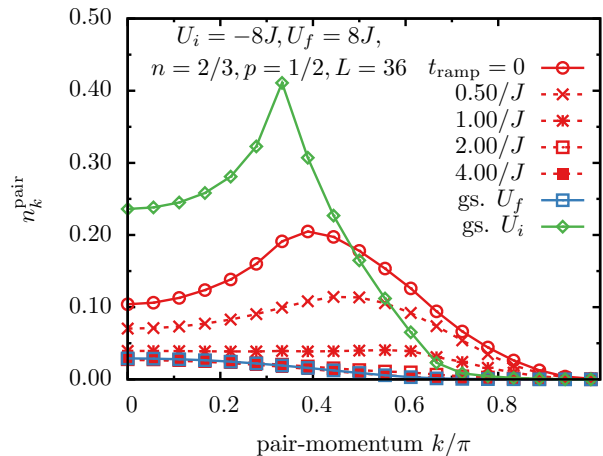


FIG. 14. (Color online) Time average of the pair-momentum distribution n_k^{pair} (calculated for $t > 4/J$) after ramps from attractive interactions ($U_i < 0$) to repulsive interactions $U_f = |U_i| > 0$, for different ramp times t_{ramp} (symbols with dashed lines). We also include results for the instantaneous quench (circles), the ground state of the attractive system at U_i (diamonds), and the ground state of the repulsive system (squares) for comparison. All results are for $n = 2/3$, $p = 1/2$, and $L = 36$ (DMRG).

B. Slow quenches: Linear ramps from $U_i < 0$ to $|U_i| > 0$

In any experiment, a quench is a fast parameter change which nonetheless takes place over a finite time window, such that one has to worry about quench-type behavior versus adiabatic changes. To account for this, we investigate slow quenches with linear ramps [see Eq. (3)] from $U_i < 0$ to $U_f = -U_i$.

An example for the time average of the pair MDF (calculated after the end of the ramp) is shown in Fig. 14, for various ramp times compared to the (instantaneous) quench and the expectation values in the pre- and postquench ground state (for $U_i = -8J$). In this example, the quench already leads to a significant reduction of n_k^{pair} (circles) compared to the initial state (diamonds), and a finite ramp time further suppresses the maximum in n_k^{pair} at finite momenta, plus shifts the position of the maximum to larger values. Already at $t_{\text{ramp}} = 2/J$, the time average coincides with the postquench ground-state expectation values (compare the different curves with squares). It is interesting to note that as the ramp time increases, the resulting pair momentum distribution approaches the postquench ground-state distribution for small momenta first, in contrast to Fig. 10, where the quench is from the noninteracting to the attractive regime.

The tendency of these quenches and ramps to dominantly populate repulsively bound pairs with large momenta can be understood from the fact that the minimum of the dispersion of the (anti-)bound state is at

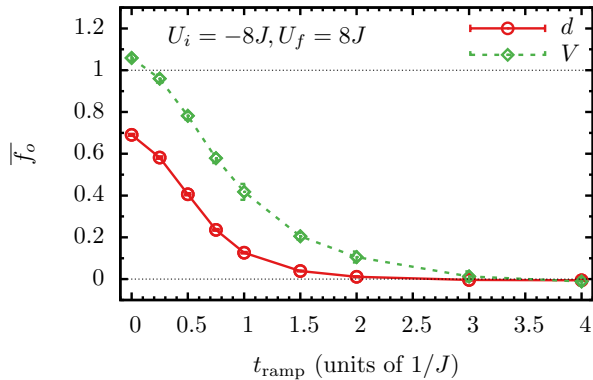


FIG. 15. (Color online) Time average of f_o [see Eq. (15)] for visibility (diamonds) and double occupancy (circles), calculated for $t > 4/J$, versus ramp time t_{ramp} after the quench and ramps from attractive $U_i < 0$ to repulsive interactions $U_f = -U_i > 0$. All data for $n = 2/3$, $p = 1/2$, and $L = 36$ (DMRG).

$k = \pi$ (compare Fig. 11). Note, though, that $k = \pi$ never gets populated; in fact, $n_{k=\pi}^{\text{pair}}$ also vanishes in the prequench state. In other words, the so-called η condensate [80, 85, 86], an exact eigenstate of the Fermi-Hubbard model with a macroscopic occupation of doublons (or pairs) at center-of-mass momentum $k = \pi$, has no overlap with our initial state.

Our results for \bar{f}_d and \bar{f}_V [see Eq. (15)] are displayed in Fig. 15, as a function of the ramp time for $U_i = -8J$, $n = 2/3$, $p = 1/2$. Both \bar{f}_d and \bar{f}_V decrease monotonously with t_{ramp} and a value of $t_{\text{ramp}} \sim 2/J$ is enough to suppress any excess pairs in the time average after the ramp, while the relative visibility f_V remains non-zero for $t_{\text{ramp}} \lesssim 3/J$ for these parameters. Note, though, that the maximum of n_k^{pair} is not necessarily at $k = q$ in the postquench state [see Fig. 14].

V. SUMMARY AND CONCLUSION

In this work we have presented an extensive numerical analysis of quantum quenches and linear ramps of the interaction strength in the 1D Fermi-Hubbard model. We are particularly interested in quenches that involve the FFLO state: we have considered quenches from the non-interacting case to negative values of U at finite spin imbalances as well as quenches from negative to positive U .

For the first example, we present results for the double occupancy and the pair MDF. We highlight four key observations: (i) The time average of the postquench double occupancy takes a maximum at $|U_f|/J \sim 4$; (ii) there are parameter regimes where the relaxation towards the steady state is exponential; (iii) the emergence of FFLO correlations in the postquench state leaves clear finger-

prints in the pair MDF; and (iv) we further demonstrate that linear ramps with ramp times of $3/J$ are sufficient to be essentially adiabatic. These aspects should, in principle, be accessible in experiments. The current obstacle is that an experimental measurement of the pair momentum distribution has not yet been accomplished for 1D quantum gases. The measurement of the double occupancy is a well-established technique.

In the second part of the paper, where we consider quenches from negative to positive values of the interaction strength, we have demonstrated that FFLO correlations can be imprinted onto repulsively bound pairs if the postquench interaction strength is high. This generates a metastable state due to the exponentially long life-time of doublons generated in such quenches [80]. In linear ramps, one quickly approaches the adiabatic case with ramp times as short as $t_{\text{ramp}} \sim 2/J$ and FFLO signatures are rapidly lost.

There are several interesting extensions of our work. For instance, for quenches of a spin-imbalanced gas from $U = 0$ to $U < 0$ in an inhomogeneous system such as realized in a harmonic trap, there need to be macroscopic spin currents in the dynamical emergence of the shell structures characteristic of a 1D spin-imbalanced Fermi gas with attractive contact interactions [13, 14, 17, 20, 87]. In this system, the core of the system is partially polarized in one dimension and in the wings, it is either fully paired or fully polarized, depending on the global polarization. The small polarization regime should be the most interesting one. Such an experiment could potentially give access to the transport coefficients of such a system (see [88] for work in that direction).

To further elucidate the relaxation dynamics of the Fermi-Hubbard model, the dynamics starting from product states in real space (see, e.g., [34], [54], and [89] for first numerical results) and the time-dependent formation of a polaron constitute potentially very instructive limiting cases for future studies.

For the question of thermalization in the Fermi-Hubbard model, where in general one would expect thermalization with respect to the generalized Gibbs ensemble because of the integrability of the model [43], at present the complicated structure of the integrals of motion presents an obstacle for testing this conjecture. The effect of integrability breaking can, in experiments, be studied either by using two-leg ladders [90], realized with superlattices [91], in fermionic superfluids with resonant interactions [92, 93], or with mass-imbalanced systems, realizable with two-component gases of different fermionic species (see the discussion in [94–98]) or using spin-dependent optical lattices [99]. A recent study [100] discussed quasi-many-body localization in such a system.

Acknowledgment. We thank F. Essler, J.-N. Fuchs, L. Radzihovsky, and W. Zwerger for helpful discussions and we thank S. Kehrein for comments on an early version of the manuscript. We further thank C. A. Büsser for his contributions at early stages of the project. F. H.-M.

was supported by the Deutsche Forschungsgemeinschaft

through DFG Research Unit FOR 801.

-
- [1] G. Sarma, *Phys. Chem. Solids* **24**, 1029 (1963).
- [2] P. Fulde and A. Ferrell, *Phys. Rev.* **135**, A550 (1964).
- [3] A. Larkin and Y. Ovchinnikov, *Zh. Eksp. Teor. Fiz* **47**, 1136 (1964).
- [4] D. E. Sheehy and L. Radzihovsky, *Ann. Phys.* **322**, 1790 (2007).
- [5] F. Chevy and C. Mora, *Rep. Prog. Phys* **73**, 112401 (2010).
- [6] K. Gubbels and H. Stoof, *Phys. Rep.* **525**, 255 (2013).
- [7] H. A. Radovan, N. A. Fortune, T. P. Murphy, S. T. Hannahs, E. C. Palm, S. W. Tozer, and D. Hall, *Nature* **425**, 51 (2003).
- [8] S. Uji, T. Terashima, M. Nishimura, Y. Takahide, T. Konoike, K. Enomoto, H. Cui, H. Kobayashi, A. Kobayashi, H. Tanaka, et al., *Phys. Rev. Lett.* **97**, 157001 (2006).
- [9] R. Casalbuoni and G. Nardulli, *Rev. Mod. Phys.* **76**, 263 (2004).
- [10] A. E. Feiguin, F. Heidrich-Meisner, G. Orso, and W. Zwerger, *Lect. Notes Phys.* **836**, 503 (2012).
- [11] X.-W. Guan, M. T. Batchelor, and C. Lee, *Rev. Mod. Phys.* **85**, 1633 (2013).
- [12] Y.-A. Liao, A. S. C. Rittner, T. Paprotta, W. Li, G. B. Partridge, R. G. Hulet, S. K. Baur, and E. J. Mueller, *Nature* **467**, 567 (2010).
- [13] G. Orso, *Phys. Rev. Lett.* **98**, 070402 (2007).
- [14] H. Hu, X.-J. Liu, and P. D. Drummond, *Phys. Rev. Lett.* **98**, 070403 (2007).
- [15] P. Kakashvili and C. J. Bolech, *Phys. Rev. A* **79**, 041603 (2009).
- [16] K. Yang, *Phys. Rev. B* **63**, 140511 (2001).
- [17] A. E. Feiguin and F. Heidrich-Meisner, *Phys. Rev. B* **76**, 220508(R) (2007).
- [18] G. G. Batrouni, M. H. Huntley, V. G. Rousseau, and R. T. Scalettar, *Phys. Rev. Lett.* **100**, 116405 (2008).
- [19] M. Tezuka and M. Ueda, *Phys. Rev. Lett.* **100**, 110403 (2008).
- [20] M. Casula, D. M. Ceperley, and E. J. Mueller, *Phys. Rev. A* **78**, 033607 (2008).
- [21] A. Lüscher, R. M. Noack, and A. M. Läuchli, *Phys. Rev. A* **78**, 013637 (2008).
- [22] M. R. Bakhtiari, M. J. Leskinen, and P. Törmä, *Phys. Rev. Lett.* **101**, 120404 (2008).
- [23] T. Roscilde, M. Rodriguez, K. Eckert, O. Romero-Isart, M. Lewenstein, E. Polzik, and A. Sanpera, *New. J. Phys.* **11**, 055041 (2009).
- [24] J. M. Edge and N. R. Cooper, *Phys. Rev. Lett.* **103**, 065301 (2009).
- [25] J. Kajala, F. Massel, and P. Törmä, *Phys. Rev. A* **84**, 041601 (2011).
- [26] C. J. Bolech, F. Heidrich-Meisner, S. Langer, I. P. McCulloch, G. Orso, and M. Rigol, *Phys. Rev. Lett.* **109**, 110602 (2012).
- [27] H. Lu, L. O. Baksmaty, C. J. Bolech, and H. Pu, *Phys. Rev. Lett.* **108**, 225302 (2012).
- [28] U. Schneider, L. Hackermüller, S. Will, T. Best, I. Bloch, T. A. Costi, R. W. Helmes, D. Rasch, and A. Rosch, *Science* **322**, 1520 (2008).
- [29] R. Jördens, N. Strohmaier, K. Günter, H. Moritz, and T. Esslinger, *Nature (London)* **455**, 204 (2008).
- [30] R. A. Hart, P. M. Duarte, T.-L. Yang, X. Liu, T. Paiva, E. Khatami, R. T. Scalettar, N. Trivedi, D. A. Huse, and R. G. Hulet, *Nature* **519**, 211 (2015).
- [31] T. Kinoshita, T. Wenger, and S. D. Weiss, *Nature (London)* **440**, 900 (2006).
- [32] S. Hofferberth, I. Lesanovsky, B. Fischer, T. Schumm, and J. Schmiedmayer, *Nature (London)* **449**, 324 (2007).
- [33] C. Kasztelan, S. Trotzky, Y.-A. Chen, I. Bloch, I. P. McCulloch, U. Schollwöck, and G. Orso, *Phys. Rev. Lett.* **106**, 155302 (2011).
- [34] S. Trotzky, Y.-A. Chen, A. Flesch, I. P. McCulloch, U. Schollwöck, J. Eisert, and I. Bloch, *Nature Phys.* **8**, 325 (2012).
- [35] M. Gring, M. Kuhnert, T. Langen, T. Kitagawa, B. Rauer, M. Schreitl, I. Mazets, D. A. Smith, E. Demler, and J. Schmiedmayer, *Science* **337**, 6100 (2012).
- [36] M. Cheneau, P. Barmettler, D. Poletti, M. Endres, P. Schauß, T. Fukuhara, C. Gross, I. Bloch, C. Kollath, and S. Kuhr, *Nature (London)* **481**, 484 (2012).
- [37] J. P. Ronzheimer, M. Schreiber, S. Braun, S. S. Hodgman, S. Langer, I. P. McCulloch, F. Heidrich-Meisner, I. Bloch, and U. Schneider, *Phys. Rev. Lett.* **110**, 205301 (2013).
- [38] T. Langen, R. Geiger, M. Kuhnert, B. Rauer, and J. Schmiedmayer, *Nature Phys.* **9**, 640 (2013).
- [39] M. Rigol, V. Dunjko, and M. Olshanii, *Nature (London)* **452**, 854 (2008).
- [40] A. Polkovnikov, K. Sengupta, A. Silva, and M. Venugalattore, *Rev. Mod. Phys* **83**, 863 (2011).
- [41] J. Eisert, M. Friesdorf, and C. Gogolin, *Nature Phys.* **11**, 124 (2015).
- [42] T. Langen, R. Geiger, and J. Schmiedmayer, p. arXiv:1408.6377 (unpublished).
- [43] M. Rigol, V. Dunjko, V. Yurovsky, and M. Olshanii, *Phys. Rev. Lett.* **98**, 050405 (2007).
- [44] F. H. L. Essler, S. Evangelisti, and M. Fagotti, *Phys. Rev. Lett.* **109**, 247206 (2012).
- [45] J.-S. Caux and R. M. Konik, *Phys. Rev. Lett.* **109**, 175301 (2012).
- [46] M. Mierzejewski, P. Prelovšek, and T. Prosen, *Phys. Rev. Lett.* **113**, 020602 (2014).
- [47] B. Wouters, J. De Nardis, M. Brockmann, D. Fioretto, M. Rigol, and J.-S. Caux, *Phys. Rev. Lett.* **113**, 117202 (2014).
- [48] B. Pozsgay, M. Mestyán, M. A. Werner, M. Kormos, G. Zaránd, and G. Takács, *Phys. Rev. Lett.* **113**, 117203 (2014).
- [49] G. Goldstein and N. Andrei, *Phys. Rev. A* **90**, 043625 (2014).
- [50] V. Alba, p. arXiv:1409.6096 (unpublished).
- [51] N. Strohmaier, D. Greif, R. Jördens, L. Tarruell, H. Moritz, T. Esslinger, R. Sensarma, D. Pekker, E. Altman, and E. Demler, *Phys. Rev. Lett.* **104**, 080401 (2010).
- [52] U. Schneider, L. Hackermüller, J. P. Ronzheimer,

- S. Will, S. Braun, T. Best, I. Bloch, E. Demler, S. Mandt, D. Rasch, et al., *Nature Phys.* **8**, 213 (2012).
- [53] S. Will, D. Iyer, and M. Rigol, *Nature Commun.* **6**, 6009 (2015).
- [54] D. Pertot, A. Sheikhan, E. Cocchi, L. A. Miller, J. E. Bohn, M. Koschorreck, M. Köhl, and C. Kollath, *Phys. Rev. Lett.* **113**, 170403 (2014).
- [55] S. R. Manmana, A. Muramatsu, and R. M. Noack, *AIP Conf. Proc.* **789**, 269 (2005).
- [56] A. Sandvik, *AIP Conf. Proc.* **1297**, 135 (2010).
- [57] G. Vidal, *Phys. Rev. Lett.* **93**, 040502 (2004).
- [58] A. Daley, C. Kollath, U. Schollwöck, and G. Vidal, *J. Stat. Mech.: Theory Exp.* (2004), P04005 (2004).
- [59] S. R. White and A. E. Feiguin, *Phys. Rev. Lett.* **93**, 076401 (2004).
- [60] J.-S. Bernier, G. Roux, and C. Kollath, *Phys. Rev. Lett.* **106**, 200601 (2011).
- [61] J.-S. Bernier, D. Poletti, P. Barmettler, G. Roux, and C. Kollath, *Phys. Rev. A* **85**, 033641 (2012).
- [62] M. Moeckel and S. Kehrein, *Phys. Rev. Lett.* **100**, 175702 (2008).
- [63] M. Kollar and M. Eckstein, *Phys. Rev. A* **78**, 013626 (2008).
- [64] M. Eckstein, M. Kollar, and P. Werner, *Phys. Rev. Lett.* **103**, 056403 (2009).
- [65] M. Eckstein, M. Kollar, and P. Werner, *Phys. Rev. B* **81**, 115131 (2010).
- [66] M. Eckstein and P. Werner, *Phys. Rev. B* **84**, 035122 (2011).
- [67] S. A. Hamerla and G. S. Uhrig, *Phys. Rev. B* **87**, 064304 (2013).
- [68] S. A. Hamerla and G. S. Uhrig, *Phys. Rev. B* **89**, 104301 (2014).
- [69] F. Heidrich-Meisner, S. R. Manmana, M. Rigol, A. Muramatsu, A. E. Feiguin, and E. Dagotto, *Phys. Rev. A* **80**, 041603 (2009).
- [70] S. Keßler, I. P. McCulloch, and F. Marquardt, *New J. Phys.* **15**, 053043 (2013).
- [71] J. Kajala, F. Massel, and P. Törmä, *Phys. Rev. Lett.* **106**, 206401 (2011).
- [72] I. Bloch, J. Dalibard, and W. Zwerger, *Rev. Mod. Phys.* **80**, 885 (2008).
- [73] U. Schollwöck, *Ann. Phys. (N.Y.)* **326**, 96 (2011).
- [74] U. Schollwöck, *Rev. Mod. Phys.* **77**, 259 (2005).
- [75] S. Sorg, L. Vidmar, L. Pollet, and F. Heidrich-Meisner, *Phys. Rev. A* **90**, 033606 (2014).
- [76] M. Greiner, O. Mandel, T. Hänsch, and I. Bloch, *Nature (London)* **419**, 51 (2002).
- [77] D. Iyer, R. Mondaini, S. Will, and M. Rigol, *Phys. Rev. A* **90**, 031602 (2014).
- [78] D. Iyer, H. Guan, and N. Andrei, *Phys. Rev. A* **87**, 053628 (2013).
- [79] K. Winkler, G. Thalhammer, F. Lang, R. Grimm, J. H. Denschlag, A. J. Daley, A. Kantian, H. P. Bahler, and P. Zoller, *Nature* **441**, 853 (2006).
- [80] A. Rosch, D. Rasch, B. Binz, and M. Vojta, *Phys. Rev. Lett.* **101**, 265301 (2008).
- [81] D. Muth, D. Petrosyan, and M. Fleischhauer, *Phys. Rev. A* **85**, 013615 (2012).
- [82] L. Xia, L. A. Zundel, J. Carrasquilla, A. Reinhard, J. M. Wilson, M. Rigol, and D. S. Weiss, *Nature Phys.* **11**, 316 (2015).
- [83] K. A. Al-Hassanieh, F. A. Reboledo, A. E. Feiguin, I. González, and E. Dagotto, *Phys. Rev. Lett.* **100**, 166403 (2008).
- [84] C. Kollath, A. M. Läuchli, and E. Altman, *Phys. Rev. Lett.* **98**, 180601 (2007).
- [85] C. N. Yang, *Phys. Rev. Lett.* **63**, 2144 (1989).
- [86] A. Kantian, A. J. Daley, and P. Zoller, *Phys. Rev. Lett.* **104**, 240406 (2010).
- [87] F. Heidrich-Meisner, G. Orso, and A. E. Feiguin, *Phys. Rev. A* **81**, 053602 (2010).
- [88] M. Tezuka and M. Ueda, *New J. Phys.* **12**, 055029 (2010).
- [89] L. Vidmar, S. Langer, I. P. McCulloch, U. Schneider, U. Schollwöck, and F. Heidrich-Meisner, *Phys. Rev. B* **88**, 235117 (2013).
- [90] A. E. Feiguin and F. Heidrich-Meisner, *Phys. Rev. Lett.* **102**, 076403 (2009).
- [91] S. Foelling, S. Trotzky, P. Cheinet, M. Feld, R. Saers, A. Widera, T. Mueller, and I. Bloch, *Nature* **448**, 1029 (2007).
- [92] S. K. Baur, J. Shumway, and E. J. Mueller, *Phys. Rev. A* **81**, 033628 (2010).
- [93] F. Heidrich-Meisner, A. E. Feiguin, U. Schollwöck, and W. Zwerger, *Phys. Rev. A* **81**, 023629 (2010).
- [94] G. G. Batrouni, M. Wolak, F. Hebert, and V. Rousseau, *Europhys. Lett.* **86**, 47006 (2009).
- [95] B. Wang, H.-D. Chen, and S. Das Sarma, *Phys. Rev. A* **79**, 051604(R) (2009).
- [96] G. Orso, E. Burovski, and T. Jolicoeur, *Phys. Rev. Lett.* **104**, 065301 (2010).
- [97] G. Roux, E. Burovski, and T. Jolicoeur, *Phys. Rev. A* **83**, 053618 (2011).
- [98] M. Dalmonte, K. Dieckmann, T. Roscilde, C. Hartl, A. E. Feiguin, U. Schollwöck, and F. Heidrich-Meisner, *Phys. Rev. A* **85**, 063608 (2012).
- [99] O. Mandel, M. Greiner, A. Widera, T. Rom, T. W. Hänsch, and I. Bloch, *Phys. Rev. Lett.* **91**, 010407 (2003).
- [100] N. Y. Yao, C. R. Laumann, J. I. Cirac, M. D. Lukin, and J. E. Moore, p. arXiv:1410.7407 (unpublished).